mobilization and neoplastic transformation[4]. However, HepG2 is aberrant expression of connexin protein and is deficient in GJIC. In the liver, connexin32 (Cx32) is the major gap junction protein expressed in hepatocytes, therefore, the aim of this study is focused on enhancing GJIC and improving liver-specific functions of HepG2 by Cx32 gene transfection.

Key word: Bioartificial liver, Connexin, Hepatoma cell

2. Materials and Methods

2.1. Cell culture

The human hepatoma cell lines HepG2 from the Riken cell bank (Tokyo, Japan) was cultured at 37℃ under 5% CO_2 / 95% humidified air using Minimum Essential Medium (MEM) (Nissui Pharmaceutical Co., Ltd., Tokyo, Japan) containing 0.1mM non-essential amino acids (NEAA) (Gibco), 10% fetal bovine serum (FBS) (Intergen Co., NY.) and 100U/ml Penicillin-Streptomycin (Gibco).

2.2. Plasmid construction and transfection

The connexin gene fragments amplified by polymerase chain reaction were isolated and inserted into the pTARGET™ mammalian expression system. HepG2 cells were transfected with the Cx/pTARGET™ plasmid DNA using FuGENE6 transfection reagent according to manufacturer's instruction with minor modification, cells transfected with empty vector as a control. After continuously culturing for two days, transfectants were selected by adding geneticin (Life Technologies, Inc., Frederick, MD) in the culture medium for one week. Individual transfected clones were prepared by limiting dilution cloning in 96-well plates, and then cultured as same as the HepG2.

2.3. Immunocytochemical stainings

Immunocytochemical staining of Cx32 protein was performed using the VECTASTAIN ABC kit in manufacturer's instruction with some modification. Briefly, cells grown on the glass cover slips were fixed in cold pure acetone for 5 min. The acetone-fixed specimens were blocked in diluted normal blocking serum in Dulbecco's phosphate buffered saline (PBS) at room temperature for 30min, and incubated with polyclonal rabbit anti-connexin32 (Zymed Laboratories Inc., San Francisco, CA) over night at 4 ℃ . Protein-antibody complexes were visualized by the biotin/streptoavidin/peroxidase method with diaminobenzidine tetrahydrochloride (DAB) as the chromogen (Vextor Laboratories, Burlingame, USA). All slides were viewed with a Nikon microscope (Nikon, Japan).

2.4. Scrape-loading dye transfer (SLDT) assay for measurement of GJIC

The SLDT technique was adapted after the method of El-Fouly et al. [5]. Briefly, when the cells grew into confluent monolayer cells in 35-cm dishes, cell dishes were loaded with 0.05% Lucifer Yellow (Molecular Probes, Eugene, OR, USA) in PBS (+) solution and were scraped immediately with a sharp blade after rinsing with PBS (+). Then incubating for 5 min at 37℃, cells were washed with PBS (+) and monitored using fluorescence microscope. The distance of the dye spreading was measured from the cell layer at the scrape to the edge of the dye front that was visually detectable.

2.5. Liver-specific function assay

The functions of the HepG2 and Cx32 transfected cells were evaluated by measuring ammonia removal and albumin secretion. For the ammonia removal activities of these cells, the cells were cultured in MEM medium with 5mM ammonium chloride. After the exchange of the medium containing ammonium, the concentration of ammonia in the medium was measured at 0 and 24hrs, respectively, using the indophenol method (an ammonia assay kit, Wako Pure Chem., Japan).

2.6. Statistical analysis

Student's t-test was used to compare the samples. Statisticall significance was represented by $p<0.05$. Date were indicated as the mean$\pm$S.D (Standard Daviation). Three cultures were run for each case, and all experiments were repeated at least twice.

3. Results and Discussion

3.1. Functional GJIC in HepG2 enhanced by Cx32 gene transfection

HepG2 cells were transfected with Cx32/pTARGET^{TM} plasmid DNA using FuGENE6 transfection reagent, and the transfectants were obtained by selection with geneticin. Enhanced expression of Cx32 mRNA was confirmed by RT-PCR (date not shown). The abilities of GJIC in Cx32 plasmid DNA transfectants were investigated by the scrape-loading dye transfer technique. Lucifer yellow, a molecular probe with low molecular weight, can diffuses in the neighboring cells through the gap junction, but not transmits from intact plasma membranes. Therefore, the transfer distances of lucifer yellow reflect the functional GJIC in the cells, and the longer distance shows the higher functional GJIC in the cells. The transfer distance of lucifer yellow in Cx32 gene transfected cells was longer than those of HepG2 and empty vector transfected cells. Thus, the distance in Cx32 gene transfected cells was 2.8 times and 2 times as long as that of HepG2 and empty vector transfected cells, respectively. It could be concluded

that the functional GJIC in HepG2 was significantly enhanced by the Cx32 gene transfection.

3.2. Localization of Cx32 protein before and after Cx32 gene transfection

In order to confirm the contribution of Cx32 proteins for the formation of functional GJIC after the Cx32 gene transfection, the localizations of Cx32 protein in the cells were further observed by immunocytochemical staining (Fig.1). The results demonstrated that the Cx32 protein expressed in HepG2, Cx32 gene transfected cells

Fig.1. Immunocytochemical staining for Cx32 in HeG2 (A), empty vector transfected cells (B) and Cx32 gene transfected cells (C).

and empty vector transfected cells, but the localizations of Cx32 protein were obviously different among them. Thus, the Cx32 protein was localized in the cell borders and formed many small gap junction plaques in the neighboring cells transfected with Cx32 gene (Fig.1.C), however, the Cx32 protein was limited in the cytoplasm and hardly detected the gap junction plaques in the HepG2 (Fig.1.A) and empty vector transfected cells (Fig.1.B). Furthermore, the morphologies of the cells showed that Cx32 gene transfected cells grew as a monolayer with the spreading cell shape, whereas the HepG2 grew as the clusters with the spherical cell shape. Although the precise role of the cellular morphology in gap junctional channel formation between the cells is not clear at the present, the results in our study could be concluded that the traffic of Cx32 protein to the cell membrane in HepG2 was enhanced by Cx32 gene transfection and then increased the GJIC in Cx32 gene transfected cells.

3.3. Liver-specific function in HepG2 improved by Cx32 gene transfection

For determining the effect of Cx32 gene transfection on the liver-specific function in HepG2, the ammonia removal activity were continuously monitored in the HepG2, empty vector transfected cells and Cx32 gene transfected cells, respectively. Ammonia clearance, which represents the detoxification potentiality of liver, was significantly higher in the Cx32 gene transfected cells than HepG2 and empty vector transfected cells

during the 14 days. These results showed that the ammoniun metabolic activity in HepG2 related with the functional gap junctional channel composed of Cx32 proteins. It was considered that the small molecular ammonium was effectively eliminated through the gap junctional channels improved by Cx32 gene transfection in HepG2.

In conclusion, transfection of Cx32 gene increased the functional GJIC in HepG2 and enhance the activity of detoxification in the Cx32 gene transfected HepG2. It may be expected to improve the cellular function of the hepatoma cell line by Cx32 gene transfection and serve to develop an excellent biohybrid-artificial liver.

References:

1. Sussman NL, Gislason GT, Conlin CA, Kelly JH (1994) The hepatix extracorporeal liver assist device-initial clinical experience. *Artif Oegans* 18:390-396.
2. Yamashita Y, Shimada M, Tsujita E, Tanaka S, Ijima H, Nakazawa K, Sakiyama R, Fukuda J, Ueda T, Funatsu K, Sugimachi K. (2001) Polyurethane foam/spheroid culture system using human hepatoblastoma cell line (HepG2) as a possible new hybrid artificial liver. *Cell Transplantation* 10:717-722.
3. Takagi M, Fukuda N, Yoshida T. (1997) Comparison of different hepatocyte cell lines for use in a hybrid artificial liver model. *Cytotechnology* 24:39-45.
4. Marie PP, Rosanne MT, Martha JF, Robert DB, Randall JR. (2000) Liver cell-specific transcriptional regulation of connexin 32. *Biochimica et Biophysica Acta* 1491:107-122.
5. El-Fouly MH, Trosko JE, Chang CC. (1987) Scrape-loading and transfer: Arapid and simple technique to study gap junctional intercellular communication. *Exp. Cell Res*. 168:422-430.

DIFFERENT EXPRESSION OF GAP JUNCTIONAL PROTEIN CONNEXIN43 IN TWO STRAINS OF MICE AFTER ONE-MONTH IMPLANTATION OF POLY-L-LACTIC ACID

SAIFUDDIN AHMED, TOSHIE TSUCHIYA.

Division of Medical Devices, National Institute of Health Sciences, 1-18-1, Kamiyoga, Setagaya ku, Tokyo 158-8501, Japan.

Abstract. The implantation of a biomaterial often induces host inflammatory responses. Some adverse effects by the biomaterials, such as poly-L-lactic acid (PLLA) and polyurethanes (PUs) were reported in animal experiments. PLLA produced tumorigenicity in rats after long-term implantation. The purpose of this study was to determine the in vitro effect of PLAO3 (high-molecular weights of PLLA) and PU8 (PTMO/MDI/BD) on the function of the normal human dermal fibroblasts (NHDF) and the in vivo effect of PLAO3 on the function of the cells originated from the subcutaneous tissue in the two female mouse strains, BALB/cJ and SJL/J. The results with Scrape-loading and dye transfer (SLDT) assay, Western Blot and RT-PCR analysis clearly demonstrated that gap-junctional intercellular communication (GJIC) and the expression of Cx43 were significantly suppressed in PLAO3-implanted group of BALB/cJ mice in compared to the control mice. While, no significant difference was found in GJIC and the expression of mRNA level but a little bit difference was observed in the Cx43 protein expression between the SJL/J implanted and the control mice. We considered that the PLAO3 suppressed irreversibly gap junctional protein connexin43 at the earlier stage after implantation and the suppression of connexin43 gene-expression might play a vital role in the inhibition of GJIC and thus promotes the tumorigenesis.

Keywords: Poly-L-lactic acid, GJIC, Connexin43.

K. Yagasaki et al. (eds.), Animal Cell Technology: Basic & Applied Aspects, Volume13, 481-485.

1. INTRODUCTION

Some adverse effects caused by the biomaterials, such as poly-L-lactic acid (PLLA) and polyurethanes (PUs) were reported in animal experiments [1]. PLLA produced tumorigenicity in rats after long-term implantation. PUs were also used for implant applications because of their useful elastomeric properties and high tensile strength, lubricity, and good abrasion resistance. However, different kinds of PUs induced various tumor incidences in rats [2]. All tumors have been generally viewed as the outcome of disruption of the homeostatic regulation of cellular ability to response to extra-cellular signals, which trigger intra-cellular signal transduction abnormally [3]. We have hypothesized that the different tumorigenic potentials of PLLA and PUs are caused mainly by the different tumor-promoting activities of these biomaterials. In the present study, we investigated the effect of PLAO3 (a high-molecular weight PLLA) and PU8 on the normal human dermal fibroblast (NHDF). Our present results showed that the PLAO3 inhibited GJIC, whereas PU8 did not inhibit GJIC after 17 days culture on these materials. These findings inspired us to investigate the role of PLAO3 on the subcutaneous tissue of the two different responder strains of BALB/cJ and SJL/J mice.

2. MATERIALS AND METHODS

2.1. ***NHDF Cell culture:*** The NHDF cells were obtained from Asahi Techno Glass (Tokyo, Japan), and maintained in Dulbecco's modified Eagle medium (DMEM) supplemented with 10% fetal bovine serum (FBS) in a 5 % CO_2 atmosphere at 37°C.

2.2. ***Animals:*** Five-week-old female BALB/cJ and SJL/J mice were obtained from Charles River (Japan).

2.3. ***Implantation of PLAO3:*** PLAO3 (20 X 10 X 1 mm) was obtained from Shimadzu Co. Ltd., and sterilized by ethylene oxide gas prior to use. Sodium pentobarbital (4 mg/kg) was intraperitoneally administered to the mice. A dorsal incision of approximately 2 cm was made, opposite sites from the incision a subcutaneous pocket was formed by blunt dissection, and one piece of PLAO3 was placed in the pocket. The incision was closed with silk thread. In both strains, Sham's operation group served as controls. After 30 days, mice were sacrificed and subcutaneous tissues were obtained for subsequent culture.

2.4. ***Cell culture of subcutaneous tissues:*** The subcutaneous tissues were maintained in

minimum essential medium (MEM) supplemented with 10% FBS in a 5 % CO_2 atmosphere at 37°C. Cells were collected by trypsinization after adequate growth.

2.5. ***Giemsa staining:*** When cells reached confluence in tissue culture dishes, cells were fixed and stained with giemsa solution. Cells morphology was determined under an inverted light microscope.

2.6. ***Scrape-loading and dye transfer (SLDT) assay for detection of GJIC:*** Confluent monolayer cells, after rinsing with Ca^{2+} Mg^{2+} phosphate-buffered saline [PBS (+)] were loaded with 0.05% Lucifer Yellow (Molecular Probes, Eugene, OR, USA)/PBS (+) solution and scraped immediately with a sharp blade. After incubation for 5 min at 37°C, cells were washed three times with PBS (+) and the extent of dye migration length was measured using fluorescence microscope.

2.7. ***Western Blot analysis:*** Cells were lysed directly in 100 μl of lysis buffer (50 mM Tris-Hcl, pH 6.8, 2% sodium dodecyl sulfate, 1 mM phenylmethylsulfonyl fluoride). Equivalent protein samples were then prepared in 7.5 % SDS-PAGE sample buffer containing 2-ME and loaded on 7% SDS-polyacrylamide gel. After electrophoresis, the proteins were transferred to Hybond-ECL nitrocellulose membranes (Amersham Pharmacia Biotech). Cx43 protein was detected by anti-Cx43 polyclonal antibodies and ECL system.

2.8. ***RT-PCR analysis:*** Total cellular RNA was isolated from cultured cells in Trizol reagent (Life Technologies, Inc.) following the manufacturer's instructions. cDNA was synthesized from 1 μg of total RNA by reverse transcript (RT) using the First-Strand cDNA synthesis kit (Amersham Pharmacia Biotech). Amplification was performed in a volume of 25 μl containing 1 μl of cDNA, 10 pmol of each primer, 0.625 unit of *Taq* polymerase (Promega, Madison, WI, USA) and 0.2 mM of each deoxynucleotide triphosphate. The amplified product was electrophoresis using 1.5% agarose gel and visualized with SYBR Green. GAPDH gene was amplified as internal control.

3. RESULTS

NHDF cells: Giemsa staining showed that the NHDF cell cultures predominantly formed a uniform monolayer of cells. All cultures maintained the elongated shape of NHDF cells. There was no difference in morphology among the control, PLAO3 and PU8. In SLDT, the GJIC was significantly inhibited in PLAO3-exposed NHDF cells in

compared to the controls. On the contrary, no difference was observed between the PU8 implanted and the control groups.

Mouse cells: Inverted light microscopy and Giemsa staining showed that the mouse cells in cultures formed a cis-cross pattern and caused decreased contact inhibition in BALB/cJ control group (Figure 1A). On the other hand, in SJL/J control group, cells were parallel and maintained the contact inhibition (Figure 1C). All cells in the implanted groups of both the strains, showed cis-cross pattern and the cells were piled up in BALB/cJ group more than in SJL/J group (Figure 1B and 1D).

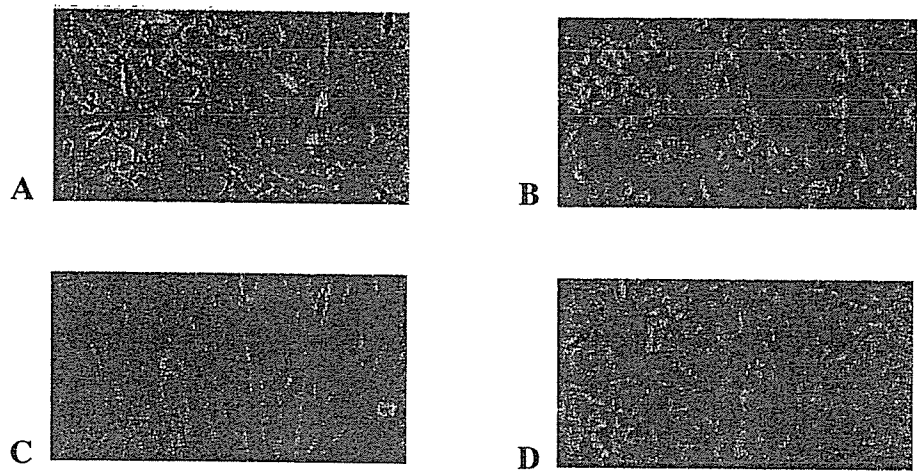

Figure 1 **Mice cells morphology. A: BAJB/cJ control, B: BALB/cJ implanted, C: SJL/J control and D: SJL/J implanted.**

In SLDT, the GJIC was significantly inhibited in PLAO3-implanted BALB/cJ cells in compared to BALB/cJ controls. No difference was observed between the PLAO3-implanted SJL/J and its controls. To clarify the cause, we also examined the mRNA and protein expression levels of connexin43 gene and found that the mRNA and protein expression were suppressed in PLAO3-implanted BALA/cJ mice in compared to BALA/cJ controls. No difference was observed between the, PLAO3-implanted SJL/J and SJL/J controls.

4. DISCUSSION

Many factors, that caused tumorigenesis were known, we especially paid attention to the inhibition of the GJIC in the PLAO3-exposed cells. PLAO3 is a widely used

biomaterial for medical and surgical implants. Gap junctions are transmembrane channels that allow the cell-cell transfer of small molecules and are composed of protein subunits known as connexin; at least 19 connexins exist and they are expressed in various kinds of tissues of rodents. Several tumor promoters have been shown to inhibit GJIC by phosphorylation modification of connexin proteins. Connexins are essential proteins to maintain the gap junctional channel [4]. To understand the mechanisms of tumorigenesis induced by PLAO3, we paid attention to the inhibitory effects on GJIC. GJIC is important for normal differentiation of the cells such as neurons and osteoblasts. In the present study, the GJIC was inhibited in PLAO3-exposed NHDF and -implanted BALB/cJ mouse cells. This perturbed gap junction is most likely to play the major role in the PLAO3-induced tumorigenesis. Our results also showed that the mRNA and protein expression of connexin43 gene were suppressed in PLAO3-implanted BALB/cJ mice. Together with these results, we speculated that the inhibitory effect of PLAO3 on GJIC might be due to the alteration in the connexin43 protein. The post-translational modification and decrease in the connexin43 protein has been shown to be involved with impaired GJIC and could be associated in tumorigenesis mechanism. All experiments will be further analyzed at 6 and 12 months after PLAO3 implantation and these experimental data will give us the basic information that are useful for understanding the adverse event induced by medical and surgical implants.

5. REFERENCE

[1] Nakamura, T. *et al.* (1994) Tumorigenicity of poly-L-lactide (PLLA) plates compared with medical-grade polyethylene, *J Biomed Mater Res.* **28**, 17-25.

[2] Xi, T. *et al.* (1994) Degradation of polyetherurethane by subcutaneous implantation into rats. I. Molecular weight change and surface morphology, *J Biomed Mater Res.* **28**, 483-490.

[3] Trosko, J.E., Madhukar, B.V. and Chang, C.C. (1993) Endogenous and exogenous modulation of gap junctional intercellular communication: toxicological and pharmacological implications, *Life Sci.* **53**, 1-19.

[4] Musil, L.S. and Goodenough, D.A. (1993) Multisubunit assembly of an integral plasma membrane channel protein, gap junction connexin43, occurs after exit from the ER, *Cell* **74**, 1065-1077.

Functionalized and Partially or Differentially Bridged Resorcin[4]arene Cavitands: Synthesis and Solid-State Structures

by **Vladimir A. Azov**[a]), **Philip J. Skinner**[a]), **Yoko Yamakoshi**[a]), **Paul Seiler**[a]), **Volker Gramlich**[b]), and **François Diederich***[a])

[a]) Laboratorium für Organische Chemie, ETH-Hönggerberg, CH-8093 Zürich (phone: (0)1 632 2992; fax: (0)1 632 11 09; e-mail: diederich@org.chem.ethz.ch)
[b]) Laboratorium für Kristallographie, ETH-Zentrum, Sonneggstrasse 5, CH-8092 Zürich

Dedicated to Professor *Duilio Arigoni* on the occasion of his 75th birthday

We report the synthesis and structural characterization of modified *Cram*-type, resorcin[4]arene-based cavitands. Two main *loci* on the cavitand backbone were selected for structural modification: the upper part (wall domain) and the lower part (legs). Synthesis of unsymmetrically bridged cavitands with different wall components (*i.e.*, **7**, **8**, and **14**–**18**) was performed by stepwise bridging of the four couples of neighboring, H-bonded OH-groups of octol **1a** (*Schemes 1*, *2*, *4*, and *5*). Cavitands with modified legs (*i.e.*, **20**, **24**, **27**, and **28**), targeted for surface immobilization, were synthesized by short routes starting from suitable aldehyde starting materials incorporating either the fully preformed leg moieties or functional precursors to the final legs (*Schemes 7–10*). The new cavitand substitution patterns described in this paper should enable the construction of a wide variety of functional architectures in the future. X-Ray crystallography afforded the characterization of cavitands **2c** (*Fig. 3*) and **24** (*Fig. 7*) in the *vase* conformation, with **2c** featuring a well-ordered CH_2Cl_2 guest molecule in its cavity. A particular highlight is the X-ray crystal-structure determination of octanitro derivative **19** (*Scheme 6*), which, for the first time, shows a cavitand, lacking substituents in the *ortho*-position to the two O-atoms of the four resorcinol moieties, in the *kite*-conformation (*Fig. 5*).

1. Introduction. – One of the most fascinating classes of receptors for chemical molecular-recognition studies comprises the resorcin[4]arene cavitands initially introduced and studied by *Cram* and co-workers [1] (*Fig. 1*). A particularly interesting property of these systems is the reversible switching between a closed *vase* conformation with a deep cavity for guest encapsulation [2] (for supramolecular

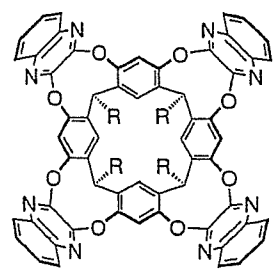

$R = C_6H_{13}$

Fig. 1. *Original resorcin[4]arene cavitand reported by* Cram *and co-workers* [1]

capsules formed by resorcinarene cavitands, see [3]) and an open *kite* conformation with a flat, extended surface. This *vase* ⇌ *kite* equilibrium is controllable by both temperature [1] or p*H* variation [4], and resembles the movement of a molecular gripper. We became interested in exploring the potential of these switchable resorcin[4]arenes for single-molecule molecular manipulation (for a first scanning/tunnelling microscopy (STM) study, imaging the *vase* conformation at molecular resolution, see [5]). Integrated into suitable devices such as scanning-probe-microscopy tips, these cavitands should be able to capture (by complexation) a single molecule in the *vase* form and hold it during translocation, while releasing it upon switching to the nonbonding *kite* conformation. To reach this objective, much diverse groundwork is required. Here, we describe the synthesis of switchable resorcin[4]arene-derived cavitands bearing legs at the lower rim for attachment to solid surfaces [5]. Partial and unsymmetrical bridging of the resorcin[4]arene bowl (for a review on resorcin[4]arenes, see [6]) greatly expands the range of dynamic cavitands. A series of derivatives bearing fluorescent 'borondipyrromethene'(BODIPY) dyes [7] attached to the upper rim of the cavitand walls were prepared for mechanistic investigations of the switching dynamics by polarization-resolved single-molecule microscopy [8] (for a preliminary report on parts of this work, see [9]). The solid-state structures of cavitands in both *vase* and *kite* conformations are also described. In a following paper [10], we will report comprehensive investigations defining the experimental conditions under which the *vase* ⇌ *kite* equilibrium of fully and partially bridged resorcin[4]arenes can be precisely addressed and studied by ^{1}H-NMR and optical spectroscopy.

2. Results and Discussion. – 2.1. *Modification of the Cavity Walls.* A variety of modifications of the cavity walls to tune the size and the inner properties of the cavitands have been reported by *Rebek* and co-workers [3][11]. Whereas most of their work involved the 'symmetric'replacement of all four quinoxaline moieties (*Fig. 1*) by four new, identical wall components, some 'unsymmetric'systems with one flap differing from the residual three have also been reported [3c,e][12]. For our planned mechanistic studies of the *vase–kite* switching process by means of single-molecule confocal fluorescence microscopy in collaboration with *B. Hecht* (University of Basel), we were interested in preparing cavitands with one or two diazaphthalimide wall flaps bearing fluorescent BODIPY dyes. Deep cavitands with the latter array of wall components had not been previously described.

On the way to the targeted cavitands, three octols **1a**–**1c** with different, solubility-providing alkyl legs were prepared from resorcinol and the appropriate aliphatic aldehydes according to a standard protocol [13] (*Scheme 1*). X-Ray-quality crystals of a solvate of the isobutyl-legged octol **1c** with two MeOH and one EtOH molecules were obtained by slow cooling of a MeOH/EtOH 4:1 solution (*Fig. 2*; for previous X-ray crystal structures of differently legged octols, see [14]). It was actually possible to grow large transparent highly solvated rhombic crystals up to several millimeters in size, they readily lost solvent upon exposure to air and disintegrated. The bowl-shaped conformation of the octol is stabilized by very short (2.64–2.77 Å) intramolecular O–H···O H-bonds (*Fig. 2,a*). Each macrocycle forms a network of intermolecular O–H···O H-bonds to a neighboring octol and to the solvent molecules included in the crystal (*Fig. 2,b*).

Scheme 1. *Synthesis of Resorcin[4]arenes* **2**–**5**

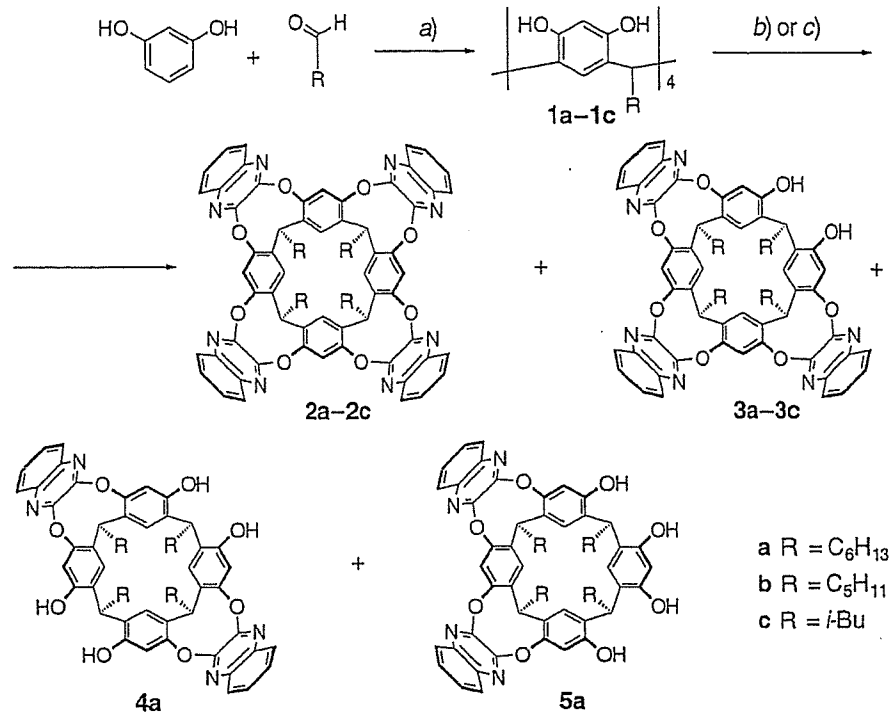

a) Conc. HCl, EtOH, 90°, 14 h. *b*) 2,3-Dichloroquinoxaline (3 equiv.), K_2CO_3, Me_2SO, 20° (8 h), then 50° (18 h); 28% (**2a**), 35% (**3a**). *c*) 2,3-Dichloroquinoxaline (2 equiv.), K_2CO_3, Me_2SO, 20° (18 h), then 50° (6 h); 2.7% (**2a**), 16.6% (**3a**), 3.2% (**4a**), 19.6% (**5a**).

The partial bridging of octol **1a** with 3 equiv. of 2,3-dichloroquinoxaline was subsequently investigated and found to be quite sensitive to the applied experimental conditions. All reactions in DMF with K_2CO_3, Cs_2CO_3, or Et_3N as a base were unsuccessful. They afforded only the fully bridged cavitand **2a** together with some tarry product; additionally, the reaction in the presence of Et_3N was very slow. In Me_2SO [2b][15], triply bridged **3a** was obtained in 30–35% yield with K_2CO_3 as base; with Cs_2CO_3, only fully bridged **2a** was formed. Starting from octols **1b** and **1c**, lower yields of the triply bridged derivatives **3b** and **3c**, respectively, were obtained besides fully bridged **2b**,**c**; therefore, octol **1a** was selected for all future bridging experiments.

Crystals of pentyl-legged **2b** as solvate with one CH_2Cl_2 and two MeCN molecules were obtained by slow evaporation from $MeCN/CH_2Cl_2$. The X-ray crystal structure shows the cavitand in the *vase* conformation (*Fig. 3*, *a*) with a C_2 axis passing through the cavity (*Fig. 3*, *b*). The CH_2Cl_2 molecule is positioned deeply within the cavity at the level of the quinoxaline N-atoms. Each Cl-atom is located above the centers of two adjacent pyrazine rings, with atom-to-ring-center distances of 3.7–3.8 Å. The disordered MeCN molecules are located one atop the cavity and the second one in the space between the four pentyl legs. In the crystal lattice, the cavitand molecules stack in a head-to-tail arrangement, forming infinite, alternating antiparallel columns (see *Fig. 6* below).

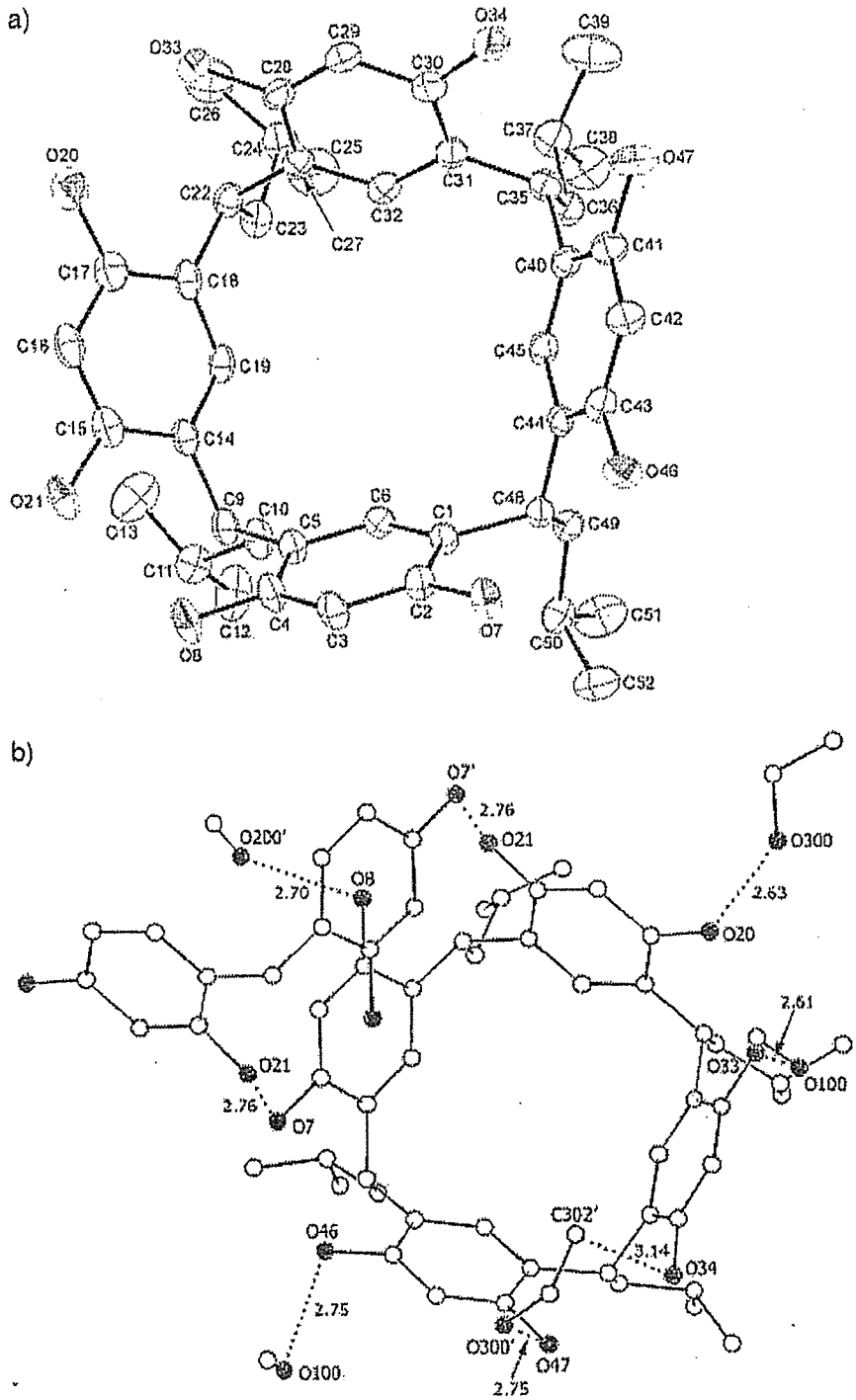

Fig. 2. a) *X-Ray crystal structure of the solvated octol* **1c** *with two MeOH and one EtOH molecules* (not shown). Arbitrary numbering. Atomic displacement parameters obtained at 233 K are drawn at the 30% probability level. Intramolecular O···O contacts [Å]: O(8)···O(21), 2.70; O(20)···O(33), 2.64; O(34)···O(47) 2.77; O(7)···O(46), 2.77. The subunit C(10)–C(13) is disordered over two orientations, here only one is shown for clarity. b) *Short intermolecular O···O contacts in the crystal packing of* **1c** *including solvent molecules and two O-atoms of the neighboring octol.* A short C–H···O interaction C(302')···O(34) is also shown. The position of O(200') is disordered over two orientations.

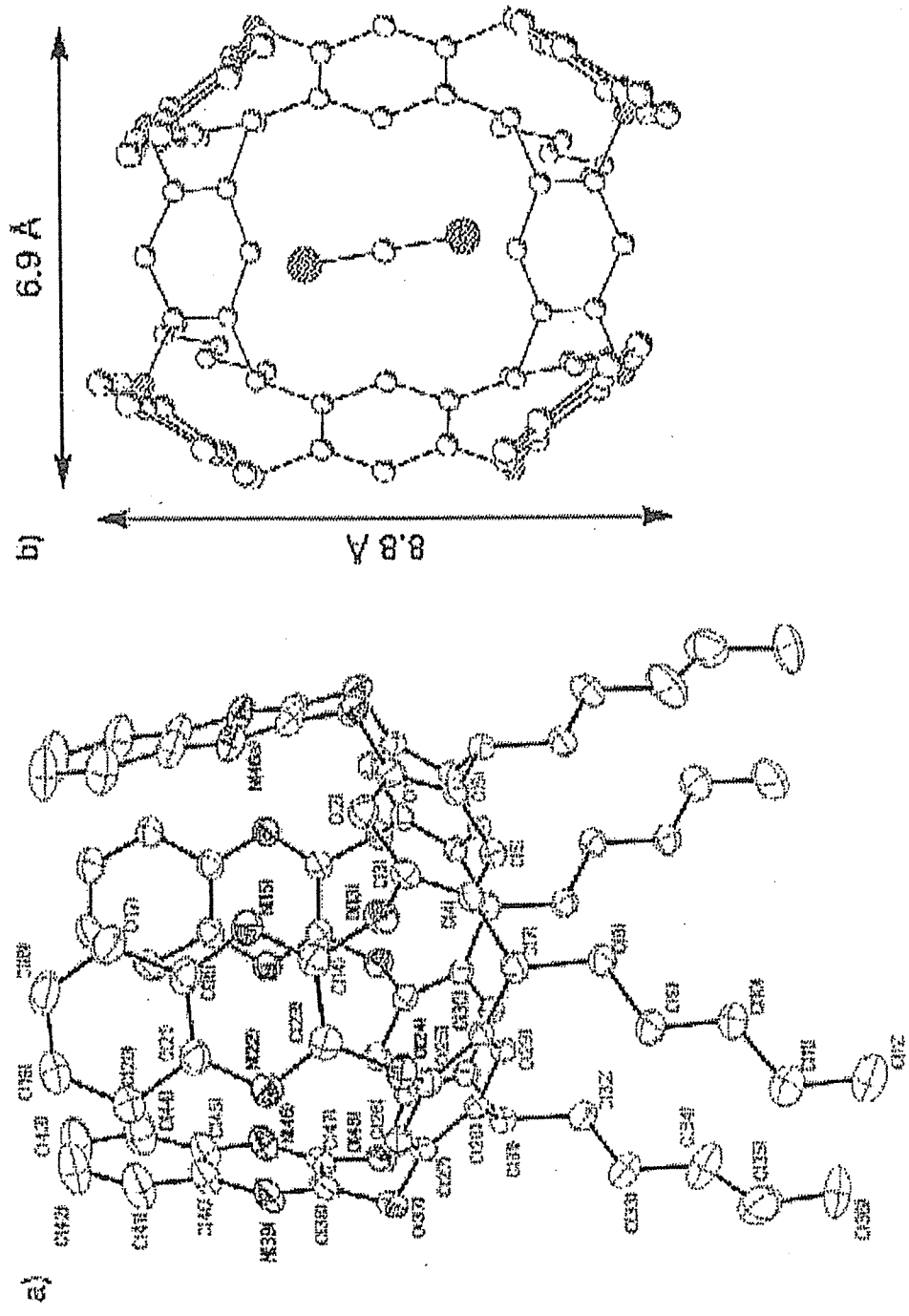

Fig. 3. a) *ORTEP Representation of the cavitand* **2b**. Arbitrary numbering. Atomic displacement parameters obtained at 295 K are drawn at the 50% probability level. Intramolecular N···N distances [Å]: N(15)···N(46a), 4.42; N(22)···N(39), 4.24. The subunit C(35)–C(36) is disordered over two orientations, here only one is shown for clarity. The CH_2Cl_2 molecule located within the cavity and two disordered MeCN molecules outside the cavity are not shown. b) *View down the* C_2 *axis into the cavity filled by the solvent.* N···Cl Distances between the Cl- and N-atoms of adjacent quinoxaline moieties range from 3.64 to 4.02 Å.

The reaction of octol **1a** with 2 equiv. of 2,3-dichloroquinoxaline (Me_2SO, K_2CO_3), followed by repeated chromatographic purification (SiO_2; CH_2Cl_2/AcOEt mixtures), afforded *anti* doubly bridged tetrol **4a** in up to 3.2% yield together with the *syn*-isomer **5a** as the major product (up to 20% yield). *Cram et al.* had previously also observed a preference for the formation of the *syn*-isomer during double bridging of an octol with methylene bridges; in fact, only the *syn*-product was isolated [16]. The chromatographic purification of the *anti*-isomer **4a** was particularly challenging due to the presence of a side product with a nearly similar retention time.

Side-products comprised structures with quinoxaline moieties attached to the octol by one ether linkage only (the structures of these colorless substances with complex NMR spectra were tentatively assigned by means of mass spectrometry (MS)) as well as colored material with a low R_f value. The latter presumably consists of products resulting from ring opening of the octol macrocycle, followed by oxidation under formation of xanthene dye-type structures [17]. Yields of the desired products increase and those of side products decrease when *i*) the starting material is freshly recrystallized and thoroughly dried under high vacuum (10^{-6} Torr) over P_2O_5, *ii*) the mixture is degassed before initiating the reaction by freeze-pump cycles, and *iii*) the reaction temperature is kept below 50°.

In a model reaction, the doubly and triply bridged octols **3a** and **5a** were transformed with dichlorodiazaphthalimide **6** into the unsymmetrically bridged cavitands **7** and **8** (*Scheme 2*). For the preparation of the bridging reagent **6**, 2,3-dichloroquinoxaline was oxidized ($KMnO_4$) to dicarboxylic acid **9** and subsequently transformed into anhydride **10** [1c]; oxalyl chloride was used instead of previously reported $SOCl_2$ as the ring-closure reagent. Heating **10** with 4-(*tert*-butyl)aniline in a small amount of Ac_2O, as reported [1c], did not prove to be very efficient, providing dichlorodiazaphthalimide **6** in only *ca.* 20% yield. On the other hand, milder conditions, with pyridine and oxalyl chloride as activation agents, afforded **6** in 86% yield. The reaction of **6** with diol **3a** and tetrol **5a** with K_2CO_3 in Me_2SO provided the fully bridged cavitands **7** and **8** in 66 and 50% yield, respectively. Neither macrocycle crystallized well; they eventually precipitated from $CHCl_3$ or THF solutions as very fine slightly yellowish powders.

For the planned single-molecule fluorescence studies, BODIPY dyes were selected as luminescent labels for their favorable electronic absorption and emission properties, and their low sensitivity to pH (which is important in proton-induced switching experiments) and environmental polarity [7]. Thus, 4-nitrobenzaldehyde was condensed with 2,4-dimethyl-3-ethylpyrrole under acidic conditions in CH_2Cl_2 to form the corresponding dipyrromethane, which was oxidized with chloranil and subsequently treated with $BF_3 \cdot OEt_2$ in the presence of Et_3N to form dye **11** in 38% yield (over the 3 steps; *Scheme 3*). Reduction of **11** (H_2, Pd/C) afforded amine **12**, which was coupled with anhydride **10** to give dichlorodiazaphthalimide **13**.

Compound **11** afforded dark-purple crystals upon slow diffusion of hexane into a $CHCl_3$ solution. The X-ray crystal structure contains three symmetry-independent molecules in the asymmetric unit with the plane of the BODIPY dye nearly orthogonal (75–87°) to the plane of the attached phenyl ring (*Fig. 4*). This should also be the case in the corresponding dye-labeled cavitands **14**–**16** (*Scheme 4*). This electronic decoupling of the π-systems ensures a very small influence of changes in the

Scheme 2. *Synthesis of the Unsymmetrically Bridged Cavitands* **7** *and* **8**

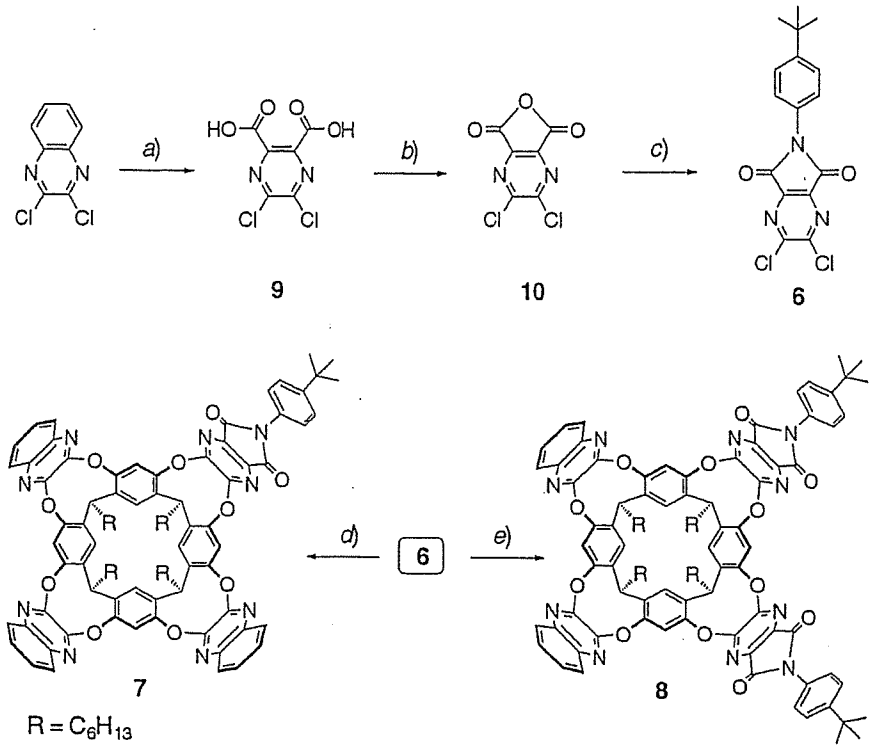

a) $KMnO_4$, H_2O, 95–97°, 2 h; 49%. *b*) $(COCl)_2$, Py (cat.), THF, 50°, 20 min; 61%. *c*) 4-(*tert*-butyl)aniline, THF, 1 h, then $(COCl)_2$, Py, 50°, 12 h; 89%. *d*) **3a** (1 equiv.), **6** (1 equiv.), K_2CO_3 (1 equiv.), Me_2SO, 20°, 24 h; 66%. *e*) **3a** (1 equiv.), **6** (2 equiv.), K_2CO_3 (2 equiv.), Me_2SO, 20°, 24 h; 50%. Py = pyridine.

Scheme 3. *Synthesis of Dichlorodiazaphthalimide* **13**

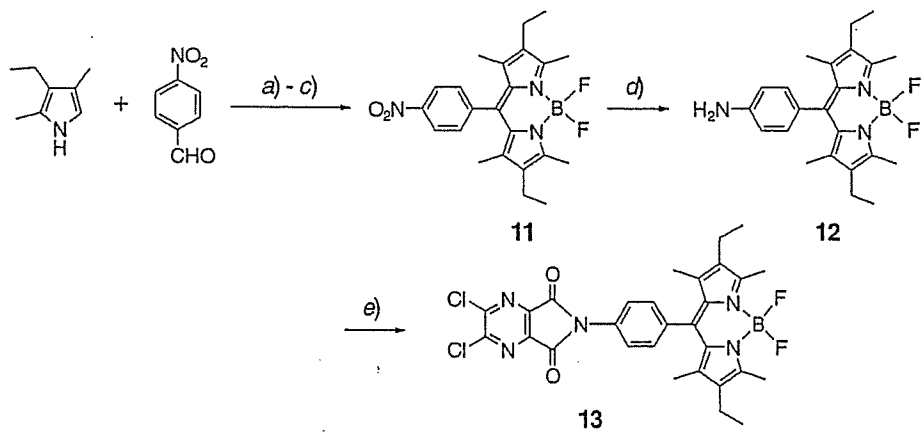

a) TFA, CH_2Cl_2, 20°, 2 h. *b*) DDQ, toluene, 1 h. *c*) NEt_3, 20° (10 min), then $BF_3 \cdot OEt_2$, 20° (30 min), then 50° (1 h); 38% (for steps *a*–*c*). *d*) H_2 (1 atm), Pd/C (10%), $CHCl_3$/EtOH 1:1, 20°, 12 h; 67%. *e*) **6**, THF, 1 h, then $(COCl)_2$, Py, 50°, 12 h; 72%. TFA = CF_3COOH, DDQ = 2,3-dichloro-5,6-dicyano-*p*-benzoquinone.

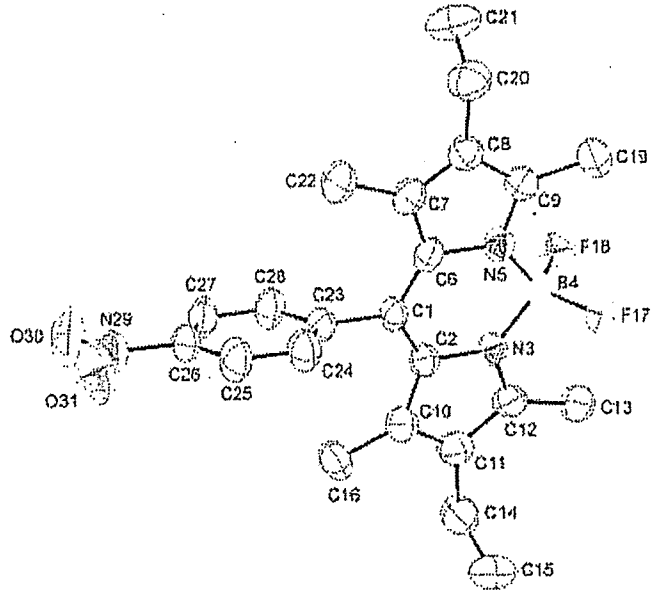

Fig. 4. *X-Ray crystal structure of BODIPY dye* **11**. Atomic displacement parameters obtained at 295 K are drawn at the 30% probability level. Only one of the three nonequivalent conformers in the elementary cell is shown.

protonation and conformation of the macrocycles on the position of the absorption and emission bands of the dye.

The BODIPY-substituted cavitands **14**–**16** were prepared from diol **3a**, and tetrols **4a** and **5a**, respectively, in 54–73% yield (*Scheme 4*). All three cavitands are brightly red-colored, featuring sharp optical absorption (530 nm) and emission (540 nm) maxima in $CHCl_3$ [9].

We also explored the introduction of different bridges into diol **3a** and tetrol **5a** by preparing the CH_2-bridged cavitands **17** and **18** (CH_2BrCl, K_2CO_3, Me_2SO; *Scheme 5*). The moderate yields (**17**: 55%; **18**: 48%) can be explained by the steric hindrance between neighboring quinoxalines, which is enhanced by the short, conformationally enforcing C_1-bridges in the cavitands. Interestingly, cavitand **18** could not be prepared starting with the corresponding *syn*-CH_2-bridged tetrol [16] and 2,3-dichloroquinoxaline.

Finally, octanitrocavitand **19** was synthesized [11a] (*Scheme 6*) to study its conformational properties. It is the first resorcin[4]arene cavitand without substituents in *ortho*-position to the two O-atoms of the four resorcinol moieties that prefers the *kite*-conformation both in solution [10] and in the solid state.

Crystals of **19** were obtained by slow evaporation from acetone solution. They quickly disintegrated in the air due to the evaporation of solvent enclathrated in the crystal lattice. Also, they shattered at temperatures below *ca.* 230 K, probably due to a phase transition. The X-ray crystal structure obtained at 253 K is remarkable. First, the cavitand is present in the *kite*-conformation (*Fig. 5,a*), which had not previously been observed for this type of resorcin[4]arene-based cavitands. Second, the cavitands do not form *face*-to-*face* dimers, as reported before by *Cram et al.* [1c,d] for velcraplexes,

Scheme 4. *Synthesis of the Dye-Labeled Cavitands* **14**–**16**

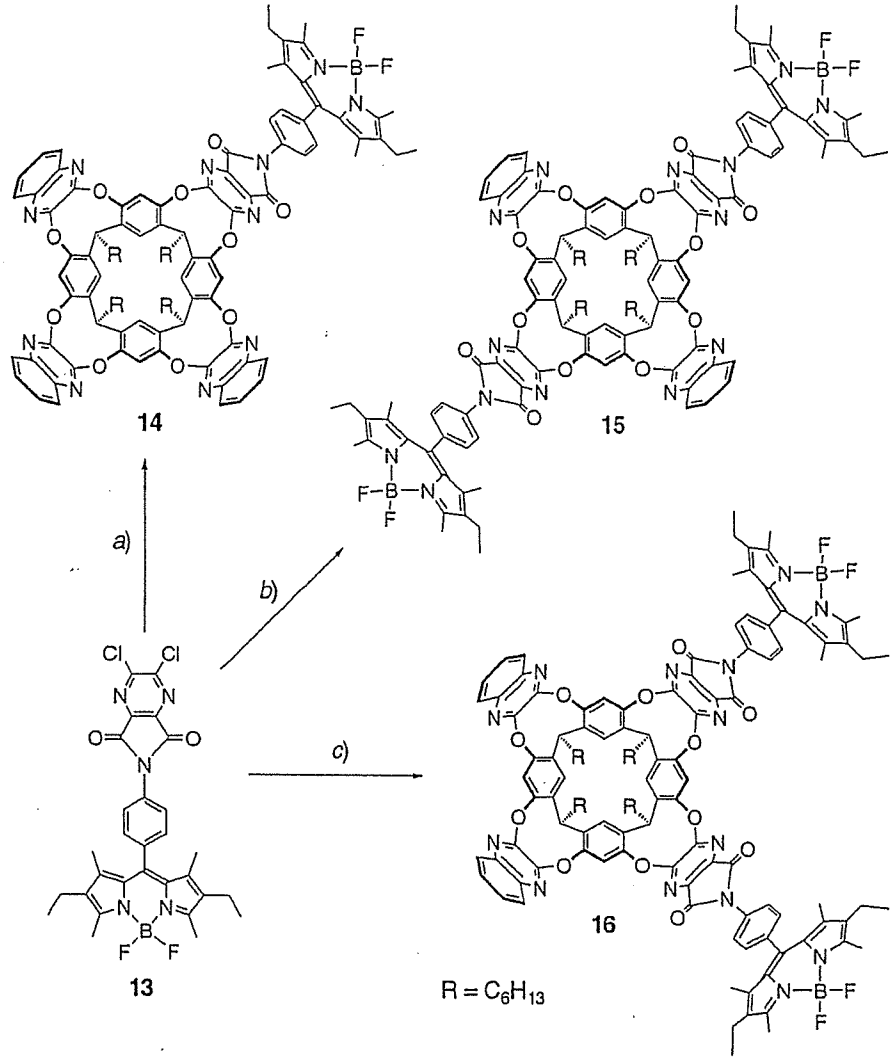

a) **3a** (1 equiv.), **13** (1 equiv.), K_2CO_3 (1 equiv.), Me_2SO, 20°, 24 h; 73%. *b*) **4a** (1 equiv.), **13** (2.2 equiv.), K_2CO_3, (2.2 equiv.), Me_2SO, 20°, 4 h, then K_2CO_3, (2.2 equiv.), 30 min; 54%. *c*) **5a** (1 equiv.), **13** (2 equiv.), K_2CO_3 (2 equiv.), Me_2SO, 20°, 24 h; 66%.

dimers of the velcrands, *i.e.*, resorcine[4]arene-based cavitands similar to those reported here but featuring Me-substituents in *ortho*-position to the two O-atoms of the four resorcinol moieties. Rather, the crystal lattice of **19** shows infinite 'head-to-tail'columns with voids filled by Me_2CO molecules (*Fig. 5,b*). We explain the preference of **19** for the *kite*-conformation with repulsive local dipole–dipole interactions between the eight NO_2 groups that approach each other closely in the *vase*-conformation. Dipolar repulsion between the NO_2 groups presumably also prevents the formation of *face*-to-*face* velcraplex-type dimers.

Scheme 5. *Synthesis of Cavitands* **17** *and* **18**

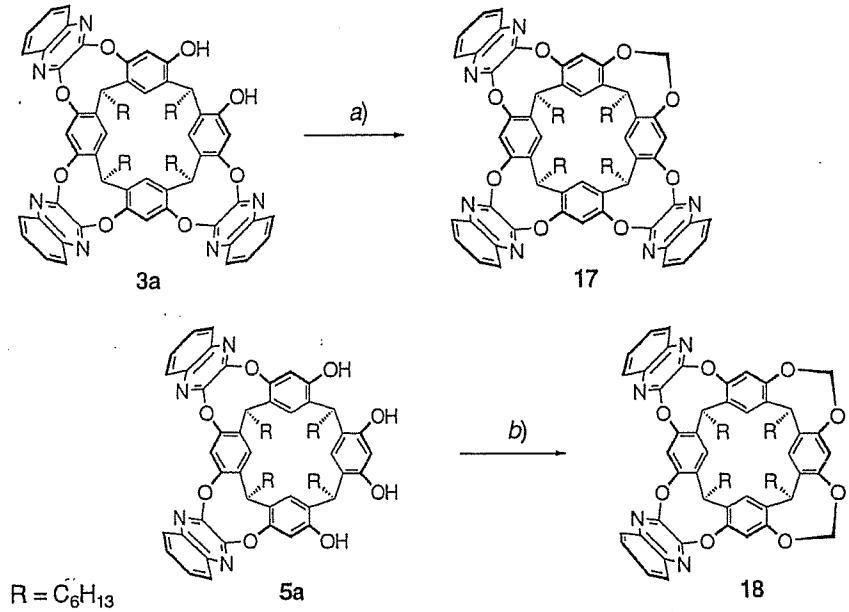

a) **3a** (1 equiv.), CH_2BrCl (4 equiv.), K_2CO_3 (2.5 equiv.), Me_2SO, 55°, 48 h; 55%. *b*) **5a** (1 equiv.), CH_2BrCl (10 equiv.), K_2CO_3 (4 equiv.), Me_2SO, 55°, 48 h; 47%.

Scheme 6. *Synthesis of the Octanitrocavitand* **19**

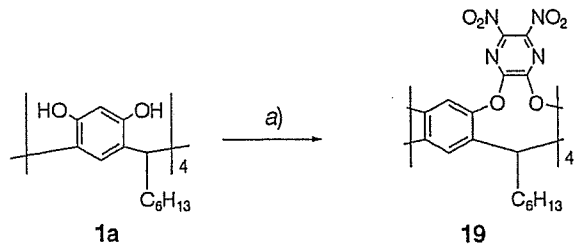

a) 1,2-Difluoro-3,4-dinitrobenzene, NEt_3, DMF, 70°, 20 h; 51%.

2.2. *Leg-Modified Cavitands.* The visualization of single cavitand molecules and the construction of practical devices require immobilization on various types of solid supports. Therefore, a substantial effort in our research program is aimed at the synthesis of cavitands suitable for surface immobilization. Previously reported modifications include the introduction of HO- [18] or NH_2-terminated legs for *i*) enhancing the solubility in aqueous media [3d], *ii*) covalent bonding to surfaces [19], and *iii*) coordination studies [20].

Cavitand **20** with four 3,5-di(*tert*-butyl)phenyl legs was prepared, since these legs had previously been shown to provide good adsorption of large molecules, such as porphyrins, on Cu surfaces for STM imaging [21]. The preparation of **20** started from 3,5-di(*tert*-butyl)phenylacetonitrile [22] that was converted *via* ester **21** into aldehyde **22** (*Scheme 7*). Acid-catalyzed condensation of **22** with resorcinol provided octol **23** in

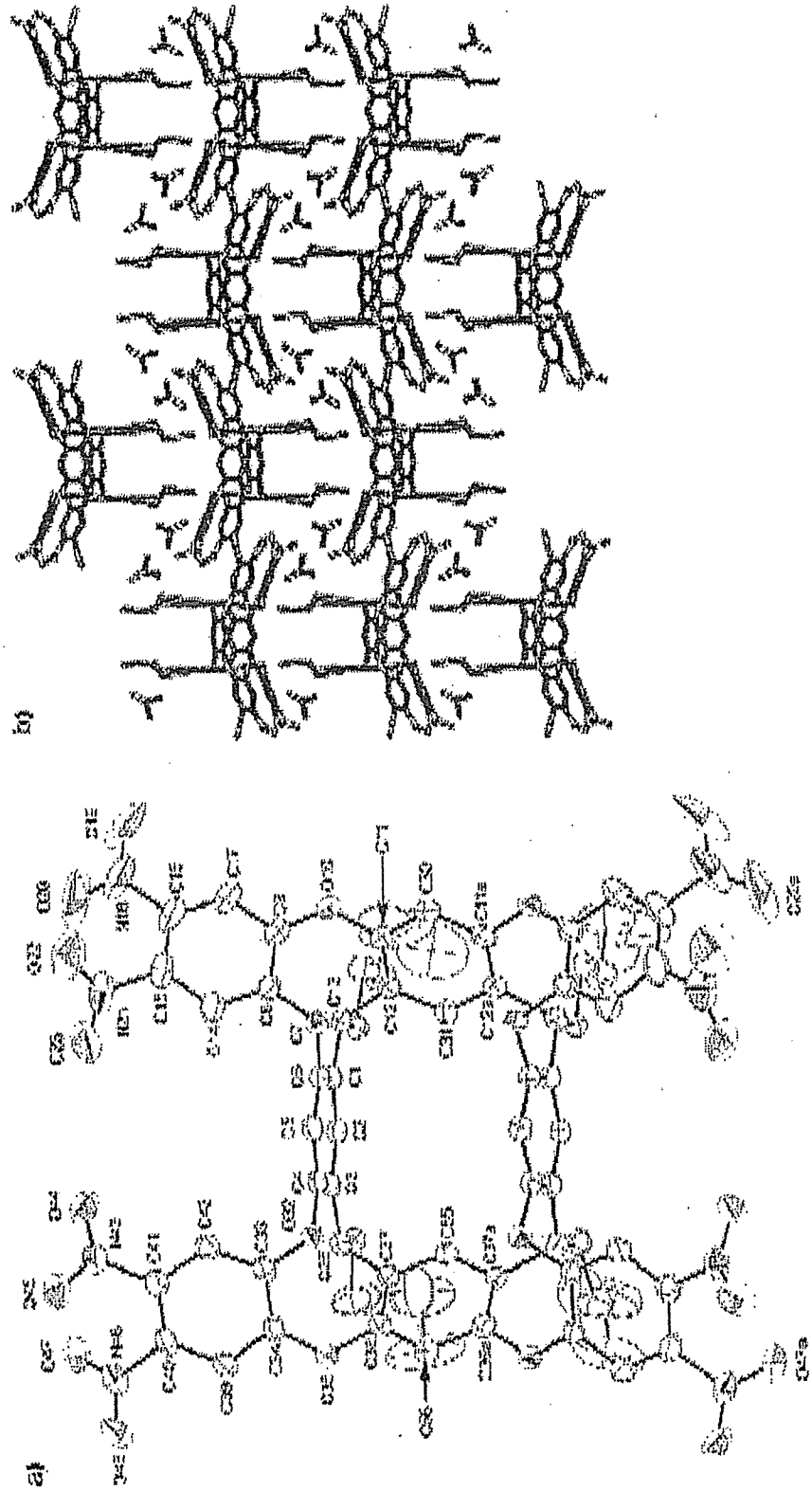

Fig. 5. a) *X-Ray crystal structure of octanitrocavitand* **19** *in a view onto the large* kite *surface.* Atomic displacement parameters obtained at 253 K are drawn at the 30% probability level. Intramolecular O ··· O distances [Å]: O(20) ··· O(20a), 15.65; O(47) ··· O(47a), 15.91; O(19) ··· O(48), 13.63. Enclathrated acetone molecules are not shown. b) *Packing diagram of* **19** *featuring columnar* head-*to*-tail *stacking.*